Final Report to the Washington Public Power Supply System

Contract C-20060

FINITE ELEMENT INVESTIGATION OF UPLIFT AND STRAIN IN THE PUGET SOUND REGION

H.J. Melosh IV

Submitted June 1 1983

1. Summary of Results

Vertical uplift and strain accumulation in the crust of western Washington state were modeled by finite element techniques. Although a full understanding of the mechanics of subduction zones still escapes science, the main features believed to characterize the Juan de Fuca-North America plate interaction were incorporated into a quasistatic plane-strain finite element code. The same code had previously been used to study subduction zone mechanics and post-seismic rebound.

The principal data constraining the results are the USGS geodetic strain measurements near Seattle (Savage et al, 1981) and the measurements of uplift by Ando and Balazs (1979). The first set of authors claim that the observed compressive strain rate of $-0.13 \pm .03\mu$ strain/yr indicates strain accumulation and the potential of large, shallow thrust earthquakes beneath the west coast of Washington. The second set of authors believe that the uplift data supports steady aseismic subduction of the Juan de Fuca plate beneath western Washington.

The finite element method allows these different hypotheses to be tested in models with realistic geometry and rheologic properties, although the full (unknown) set of forces acting on the crust cannot be exactly represented. The runs made under different conditions are sufficiently distinctive, however, to show that

(1) The observed compressive strain rate is roughly twenty times too large to be due wholly to strains associated with the uplift.

(2) Uplift rates obtained from steady subduction models are one or more orders of magnitude larger than observed. Although strain rates comparable to the USGS observations are obtained in some cases, they are invariably associated with uplift rates of $\sim$50

mm/yr, compared to observed rates of ∿3 mm/yr.

(3) Models in which strain is accumulating on a locked fault fit the data best, although these models predict a very complex pattern of uplift and strain.

Finally, a more technical result that was

(4) The bend in the subducted Juan de Fuca plate, if it exists, must be mechanically decoupled from the overriding continental lithosphere. If not, unreasonably large uplift rates develop over the bend.

The following report spells out the method used for the analysis, details of the geometry and boundary conditions, and discusses the results in more depth.

2. The Finite Element Model

2.1 The Finite Element Method

Finite element analysis is a technique that has been developed over the last 20 years for engineering analysis of complex structures (Bathe and Wilson, 1976). The continuous distribution of displacements and stresses in a structure is represented by an array of discrete displacements localized at nodes. The nodes are at vertices of elements in which displacement, stress and strain are assumed to vary in a simple fashion (usually linearly). Each element may have its own rheologic properties (elastic modulus, poisson ratio, viscosity, etc). The work described here employed three and four node isoparametric ("serendipity") elements. Assembly of a collection of nodes and elements of various sizes, shapes, and positions allows the mechanical characterization of highly complex structures. Various boundary conditions (both internal and external to the grid) may also be applied. Stresses and displacements developing as a result of the imposed boundary conditions are determined by inverting the "stiffness matrix" $\underline{K}$. This matrix is typically a large (686 x 686 in this case) banded (mean half-width 24 in this case) symmetric matrix. It is inverted by Gaussian elimination on a large computer, the U. of Arizona Cyber 175 for this investigation. The stiffness matrix relates the array of displacements $\underline{U}$ to the array of nodal forces $\underline{F}$ by

$$[\underline{K}]\ \underline{U} = \underline{F}.$$

Its inverse allows the displacements to be computed from the forces.

Details of the finite element code used for this work are described by Melosh and Raefsky (1980). The code uses an implicit-explicit quasistatic algorithm and was specifically designed for time dependent (viscoelastic) tectonic problems. Faults are introduced via an efficient "split-node"

technique described by Melosh and Raefsky (1981). Time stepping is dictated by the rheologic properties of the model. To retain high accuracy, the time step is controlled by the lowest viscosity element. This constrains the range of viscosity that can be treated in a practical run (the code is unconditionally stable in the fully implicit mode, so accuracy, not runaway displacements, are the primary concern). The nodal coordinates are fixed during a run to avoid high computer costs associated with regriding during the calculation. The results are thus inaccurate when displacements become a significant fraction of the element size. This limits the total time span the model can represent. In the runs reported here this limit was reached between 300,000 and 1,000,000 years after the run began.

2.2 Rheologic Structure of Western Washington State

Figure 1 illustrates the geologic structure chosen for finite element modeling. There are ten distinct types of material that make up the model. The properties of each material are summarized in Table 1.

The elastic properties of the material types are averages from the global PEM models of Dziewonski et al (1975). Densities are taken from the same models, with the exception of the Eclogite layer. The properties of eclogite and the thicknesses of the continental upper and lower crustal layers were derived from G.C. Rodger's (1983) compilation. The thickness of the subducted plate is taken to be 26 km (6 km oceanic crust plus 20 km upper mantle) on the basis of the Oldenberg (1975) formula,

$$\text{thickness (km)} = 9.5 \sqrt{\text{Age (Myr)}}$$

The viscosity of the oceanic low velocity zone is estimated from global models of postglacial rebound (Peltier, 1981; Walcott, 1973). The viscosity of

the continental low velocity zone (LVZ) in the western United States is taken from Passey (1981). A viscosity of 10^{22} Pa-s is assigned to both continental and oceanic upper mantle, consistent with the results of Melosh and Raefsky (1981) on the bending of plates in subduction zones.

Most of the models included a low viscosity wedge near the tip of the subducting slab. The evidence for the existence of this wedge is circumstantial, but it seems reasonable that the mantle beneath the Cascade volcanoes should be especially fluid. Wahr and Wyss (1980) showed that such a wedge near the subducting Pacific plate in Alaska could explain the uplift observed subsequent to the 1964 earthquake. The rapid timescale for postglacial rebound following melting of the Puget lobe of the continental ice sheet (Thornson, 1983) also argues for a low viscosity region in the upper mantle. Computer runs were performed both with and without this zone and little difference was found for either steady subduction or strain accumulation solutions.

The geometric properties of the finite elements model were constrained by the data of Crosson (1983). Figure 2 shows his earthquake hypocenters superimposed on the structure chosen for the finite element model. Earthquakes are mainly confined to the continental crust and oceanic crust and upper mantle. There are few earthquakes in the low viscosity wedge. Following Rodgers (1983) and other authors referenced therein, a bend in the slab was centered 40 km SW of the center of the section. The slab dips at 8.5° from the foot of the continental slope then steepens to 17° under the cascades. The earthquake data are consistent with this geometry.

The finite element model assumes plane strain and thus that the cross section extends infinitely along strike of the subduction zone. In fact, the

plate extends unchanged only a few hundred km from the section. Small scale (less than a few 100 km) features are probably correctly represented, but larger scale features of the results should not be accepted without verification by 3-D modeling.

The finite element model follows the trend of Crosson's profile, striking N60°E from a center located at 122°30'W, 47°30'N. This trend is nearly perpendicular to the subducting Juan de Fuca plate. The convergence velocity is assumed to be 4.0 cm/yr (FSAR report, 1982) The computer results on uplift and strain rates scale directly with the velocity so if, for example, the convergence velocity were 2.0 cm/yr, the uplift and strain rates reported here should be halved.

2.3 The Finite Element Grid

The finite element grid constructed to model the geometry in Figs. 1 and 2 is illustrated in Fig. 3. It extends from -1000 to +1000 km from the center to minimize edge effects in the central region. It is 420 km deeps also to prevent boundary conditions from affecting the solution. It consists of 379 nodes and 391 elements. The grid spacing is typically 20 km in the central region where stress and strain gradients are large, increasing to 80 km near the boundaries.

The specific form of the boundary conditions was shown not to significantly affect the solution (Runs 3 and 7). Displacements were fixed to zero along the entire bottom of the grid and along its vertical sides except near the top where a constant velocity was applied to the topmost two nodes, simulating motion of the Juan de Fuca and North American plates. In several runs the subducted plate was also pulled downward at constant velocity. Slip on the fault was modeled using a line of split nodes that extend from the surface into the low viscosity wedge at a depth of 53 km.

2.4 Elastic Solution

Figure 4 is a plot of the uplift due to uniform slip on the fault without viscous stress relaxation. It is qualitatively similar to the dislocation solution of Savage et al (1983) for a 10° dipping fault in a homogeneous elastic half space. The differences in detail are due to the more realistic geometry and elastic properties employed in the finite element model. The general nature of the result is that the wedge of continental crust overlying the fault is thrust upward along the inclined fault while a trough develops over a fault tip. This pattern is also qualitatively similar to the topography in the area. The coast ranges correspond to the uplifted wedge and the Puget Lowland to the trough over the fault tip.

3.0 Results of the Finite Element Models

3.1 Steady Subduction

Several runs (1, 3, 5, 7 and 8) were performed to model steady subduction of the Juan de Fuca plate in the absence of subsidence due to gravity. The results of Runs 1, 3 and 5 are illustrated in Figs. 5, 6 and 7. Run 7 differed from 3 only in the boundary conditions at the sides (horizontal displacements below the two nodes were not constrained to zero). Run 8 had no low viscosity wedge over the slab. Since the results are indistinguishable from Run 3 they are not separately illustrated.

Run 1 modeled steady symmetric convergence (2 cm/yr from either side) and steady slip on the fault. No slab pull forces were included. The uplift rates reached constant values 300 years after the start of the run and continued until the run terminated at 500,000 years. Figure 5 shows the uplift and strain rates 1177 years after the run began. The main feature is a 100 km wide zone of very rapid uplift (up to 50 mm/yr) centered in the Puget Trough. This uplift is associated with extensional strain rates of up to 80 nannostrain/year (ns/yr) under the upwarp, flanked by compressive strain regions with strain rates up to 160 ns/yr. Although this strain rate is comparable to the -130±30 ns/yr observed by Savage et al (1981), the rate and pattern of uplift violently disagrees with the results of Ando and Balazs (1979). The upwarp is centered over the bend in the slab and is evidently due to stresses that develop as the continental lithosphere overrides the bend.

Run 3 is similar to Run 1 except that slab pull forces were added. Figure 6 illustrates the uplift and strain rates for this model after 1177 yrs. Again, a very high rate of uplift develops due to the bend in the subducted slab. The results are essentially identical to Run 1.

Run 5 is similar to Run 3 except that convergence is asymmetric: the North American plate is fixed with respect to the deep mantle while the Juan de Fuca plate moves. Again, the results are essentially identical to Runs 1 and 3.

Run 10 (Fig. 8) shows what happens when the bend is decoupled from the overriding plate. The uplift rate is far lower than for the coupled solutions (reaching 9 mm/yr -- still higher than the observed range of 5 mm/yr) and the pattern is similar to that observed by Ando and Balazs (1979). The strain rates, however, do not match those observed by the USGS -- they reach a maximum of only 60 ns/yr and are extensional, not compressive, in the Puget Trough.

None of the runs described above include gravitational forces. The regional uplifts are thus not counteracted by sinking due to isostatic adjustment. To a first approximation this can be accounted for simply by altering the zero of the uplift axis, since isostatic adjustment is regional (on a scale of hundreds of kilometers) whereas the upwarps computed above are local. Thus, for example, the results of Run 10, which show no true sinking, can be brought into line with the observtion by adding an overall subsidence of few mm/yr.

Two runs were, however, performed in which gravitational forces were present. Run 2 gave uninterpretable results because of an error in applying the boundary conditions. This error was corrected in Run 6 but the results were highly unrealistic, underlining the approximate nature of the finite element model. Subsidence rates of several m/yr developed in the region overlying the subducted slab: evidently the weight of the slab was not balanced by viscous stresses in the mantle and it simply sank vertically, drawing the surface down with it. The complete pattern of flow in the mantle must be known to obtain a realistic solution, along with the exact densities of all materials, flow velocities, etc. Elucidation of such details is impossible in the present state

of our knowledge (this is an active area of research at the present time).

3.2 Strain Accumulation

Two runs were performed in which the fault was locked and strain allowed to accumulate. In both cases steady slip was allowed under the conditions of Run 3 (symmetric convergence with slab pull) until steady state was reached. Then, after 7,025 years of steady flow, the fault was locked to a depth of 29 km (the base of the continental crust). Strain accumulation reaches a steady state after only a few decades. The accompanying figures (9 and 10; 11 and 12) show uplift rates and strain rates at 67 and 320 years after locking for Runs 4 and 11, respectively. The rates at the two different times are nearly identical, indicating that a steady state of linear uplift and strain accumulation has been reached.

Run 4 includes interaction with the bend in the slab. The uplift pattern is similar to Runs 1, 3 and 5 with rapid (up to 60 mm/yr) uplift in the Puget Trough. The strain rates, however, are compressional nearly everywhere due to the accumulating strain and are consistent with the observed -130 ns/yr. Thus, the strain rates accord with the observation but the uplift rates and patterns disagree.

The bend region is decoupled in Run 11 (Figs. 11 and 12). The uplift pattern is complex with a region of uplift offshore where strains are accumulating in the overthrust wedge, then another region of uplift between the Puget Trough and the reactor site. Downwarping is observed in an area corresponding with the Puget Trough although displaced slightly eastward from it. This upwarp is produced by continued slip on the subducted part of the slab below the 29 km locking depth. The strain rate is similarly complex,

extensional strain occurring in the upwarped region between the Puget Trough and the reactor site while compressive strain (-75 to -100 ns/yr) accumulates beneath the Puget Trough.

The uplift rate computed in Run 11 is comparable to the observed rates, as is the strain rate. The results of Run 11 are thus, of all the runs, the best match to the meager observations of uplift and strain. The complexity of the strain pattern should provide a strong motivation for further measurements to either verify or rule out the model.

5. The Relation between Uplift and Strain

Uplift rates and strain rates are intimately related. In a thin elastic plate the uplift rate $\dot{W}$ is related to surface strain rate $\dot{\varepsilon}_{XX}$ by (Turcotte and Schubert, 1982, p. 115).

$$\dot{\varepsilon}_{XX} = -\frac{h}{2}\frac{d^2\dot{W}}{dX^2}$$

where h is the plate thickness. Thus extensional strain occurs beneath the crest of uplifts and compressional strain on the flanks, as computed in Run 3 and similar runs. In addition to this bending strain, horizontal strains due to convergence may also be added. They are not present in the steady subduction solutions but arise if the fault is locked.

The above formula permits an estimate of the compressive strain rate due to the observed uplift. The contours of Ando and Balazs (1979) are projected on the line of the finite element model in Figure 13. The second derivative of the uplift evaluated at the position of the USGS strain array is

$$\frac{d^2\dot{W}}{dX^2} = (2.4 \pm 1) \times 10^{-10} \text{ 1/km-yr.}$$

Taking a plate thickness of 30 km yields a compressive strain rate of

$$\dot{\varepsilon}_{XX} = -3.6 \text{ ns/yr}$$

This is a factor roughly 20 times smaller than the observed rate. The fact that Run 3 and similar runs produced strain rates comparable to that observed is simply because the uplift rates are so high in those runs: Run 10, which yielded a much lower uplift rate, also had strain rates far lower than observed.

These considerations clearly show that the observed compressive strain rate

is not due wholly to the uplift. Another component, most plausibly accumulating compressive strain, must be present.

6. Conclusions and Discussion

The finite element models computed in this investigation are unrealistic in several ways since the full set of forces and geologic processes acting in western Wastington state are not known. However, the results are sufficiently distinctive to permit a number of general conclusions that probably hold in spite of the unknowns.

(1) The compressive strain rate observed by the USGS is too large to be explained by flexure due to uplift. Another component of compressive strain must be present.

(2) None of the steady subduction models produce both uplift rates and strain rates that agree with the observations. The models in which the slab bend is coupled to the plate above produce plausible strain rates but at the cost of impossibly high uplift rates. The model in which the bend was decoupled produced plausible uplift rates but strain rates that are too small (and of the wrong sign).

(3) The best fit for both strain and uplift rate is a model in which the fault is locked (and may have been locked for hundreds of years) and the bend decoupled. The pattern of strain and uplift, however, is complex: this complexity could be tested by further observations.

It can also be noted that the bend in the slab, if it exists as postulated, must be mechanically decoupled from the overriding plate: no model with a coupled bend produced plausible uplift rates.

Finally, it should be stated that the finite element model, being a plane-strain model, predicts a zero strain rate perpendicular to the line of

section ($\dot{\varepsilon}_{ZZ} = 0$). However, Savage et al (1981) note an extensional strain rate in this direction of 70±20 ns/yr. Several explanations have been proposed, but I want to point out that the subducted slab in this region appears to be gently curved in plan (convex toward the continent) with a radius of curvature of several hundred kilometers (Rogers, 1983). If this curved slab is being bodily displaced eastward at a few (or one) cm/yr as strain accumulates, then an azimuthal strain should develop tangent to the curved slab at a rate

$$\dot{\varepsilon}_{ZZ} = \frac{V}{R}$$

where V is the velocity of displacement and R is the radius of curvature. For V = 1 cm/yr and R = 300 km, $\dot{\varepsilon}_{ZZ}$ = 66 ns/yr -- comparable with the observed rate. This extensional strain may thus be associated with the curvature of the plate and does not necessarily indicate the presence of other, unaccounted for, forces. Consistent with this idea, no tangential extensional strains are observed farther north on Vancouver island where the Juan de Fuca plate appears to be straight (Savage et al, 1981).

References

Ando, M. and Balazs, E.I. (1979) Geodetic evidence for aseismic subduction of the Juan de Fuca plate, J. Geophys. Res. 84, 3023-3028.

Bathe, K.-J. and Wilson, E.L. (1976) Numerical methods in finite elemennt analysis, Prentice-Hall, Englewood Cliffs, NJ, 528 pp.

Crosson, R.S. (1983) Review of seismicity in the Puget Sound region from 1970 through 1978: A brief summary, USGS Open File Report 83-19, 6-18.

Dziewonski, A.M, Hales, A.L., and Lapwood, E.R. (1975) Parametrically simple earth models consistent with geophysicl data, Phys. Earth Planet. Inst. 10, 12.

Melosh, H.J. and Raefsky, A. (1980) The dynamical origin of subduction zone topography, Geophys. J. R. Astr. Soc. 60, 333-354.

Melosh, H.J. and Raefsky, A. (1981) A simple and efficient method for introducing faults into finite element computations, Bull. Seis. Soc. Amer. 71, 1391-1400.

Oldenberg, D.W. (1975) A physical model for the creation of the lithospere, Geophys. J. 43, 425-451.

Passey, Q.R. (1981) Upper mantle viscosity derived from the difference in rebound of the Provo and Bonneville shorelines: Lake Bonneville Basin, Utah, J. Geophys. Res. 86, 11701-11708.

Peltier, W.R. (1981) Ice age geodynamics, Ann. Rev. Earth Planet. Sci. 9, 199-225.

Rogers, G.C. (1983) Seismotectonics of British Columbia, U. British Columbia, Ph.D. Thesis.

Savage, J.C. (1983) A dislocation model of strain accumulation and release at a

subduction zone, J. Geophys. Res., in press.

Savage, J.C., Lisowski, M., and Prescot, W.H. (1981) Geodetic strain measurements in Washington, J. Geophys. Res. 86, 4929-4940.

Thorson, R.M. (1983) Isostatic effects of the last glaciation in the Puget Lowland, Washington (Abs.), USGS Open File Report 83-19, 300-301.

Turcotte, D.L. and Schubert, G. (1982) Geodynamics, J. Wiley and Sons, NY, 450 pp.

Wahr, J. and Wyss, M. (1980) Interpretation of postseismic deformation with a viscoelastic relaxation model, J. Geophys. Res. 85, 6471-6477.

Walcott, R.I. (1973) Structure of the Earth from glacio-isostatic rebound, Ann. Rev. Earth Planet. Sci. 1, 15-37.

Figures

Figure 1. Geologic cross section of western Washington State. The profile strikes N60°E and is centered at 122°30'W, 47°,30'N.

Figure 2. Geometric structure of the finite element model superimposed on the earthquake hypocenters of Crosson (1983).

Figure 3. The finite element grid. The detail shows the grid structure in the vicinity of the profile center.

Figure 4. Elastic deformation normalized by net convergence for the finite element model. The fault extends to 53 km depth.

Figure 5. Uplift and strain rate from Run 1, 1177 years.

Figure 6. Uplift and strain rate from Run 3, 1177 years.

Figure 7. Uplift and strain rate from Run 5, 1177 years.

Figure 8. Uplift and strain rate from Run 10, 1177 years.

Figure 9. Uplift and strain rate from Run 4, 67 years.

Figure 10. Uplift and strain rate from Run 4, 320 years.

Figure 11. Uplift and strain rate from Run 11, 67 years.

Figure 12. Uplift and strain rate from Run 11, 320 years.

Figure 13. Observed uplift rates along the line of finite element grid. Replotted from Ando and Balazs (1979).

Table 1

Material Properties for the Finite Element Model

Material #	Description	Youngs Modulus 10^{11} Pa	Poisson Ratio	Density kg/m^3	Viscosity Pa-s
1	Upper Mantle (>200 km)	1.9	0.30	3500	1×10^{21}
2	Oceanic LVZ	1.6	0.28	3350	1×10^{20}
3	Continental LVZ	1.7	0.26	3400	2×10^{19}
4	Oceanic U. Mantle	1.7	0.25	3400	1×10^{22}
5	Eclogite	1.8	0.25	3500	1×10^{20}
6	Low Viscosity LVZ	1.5	0.25	3350	1×10^{18}
7	Oceanic Crust	1.0	0.25	2850	1×10^{25}
8	Continental U. Crust	0.8	0.25	2700	1×10^{25}
9	Continental L. Crust	1.0	0.25	2900	1×10^{22}
10	Continental U. Mantle	1.8	0.25	3350	1×10^{20}

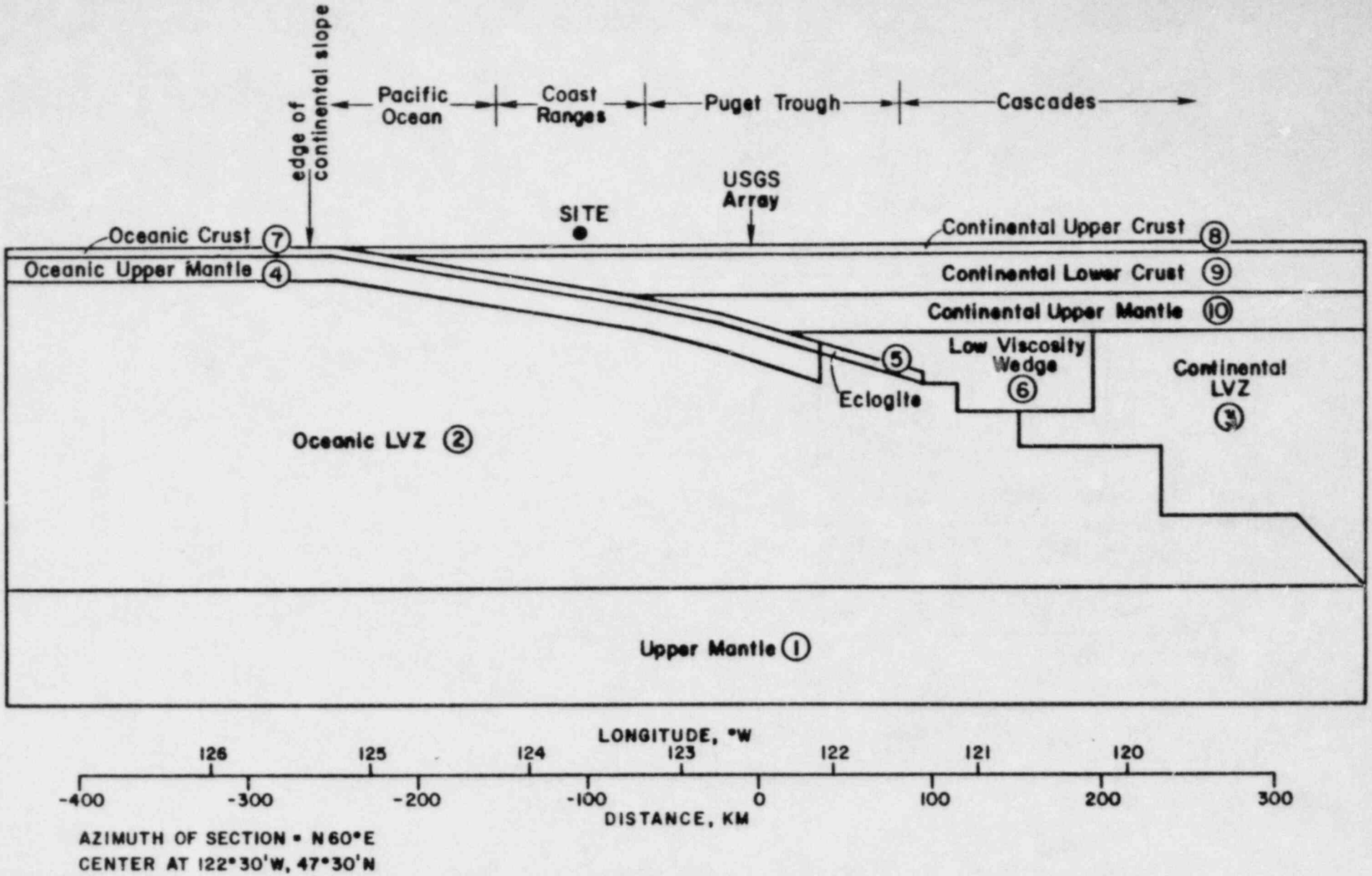
edge of continental slope
Pacific Ocean
Coast Ranges
Puget Trough
Cascades
USGS Array
SITE
Oceanic Crust 7
Oceanic Upper Mantle 4
Continental Upper Crust 8
Continental Lower Crust 9
Continental Upper Mantle 10
Low Viscosity Wedge 6
5
Eclogite
Continental LVZ 3
Oceanic LVZ 2
Upper Mantle 1
LONGITUDE, °W
126
125
124
123
122
121
120
-400
-300
-200
-100
0
100
200
300
DISTANCE, KM
AZIMUTH OF SECTION = N60°E
CENTER AT 122°30'W, 47°30'N

Fig 1

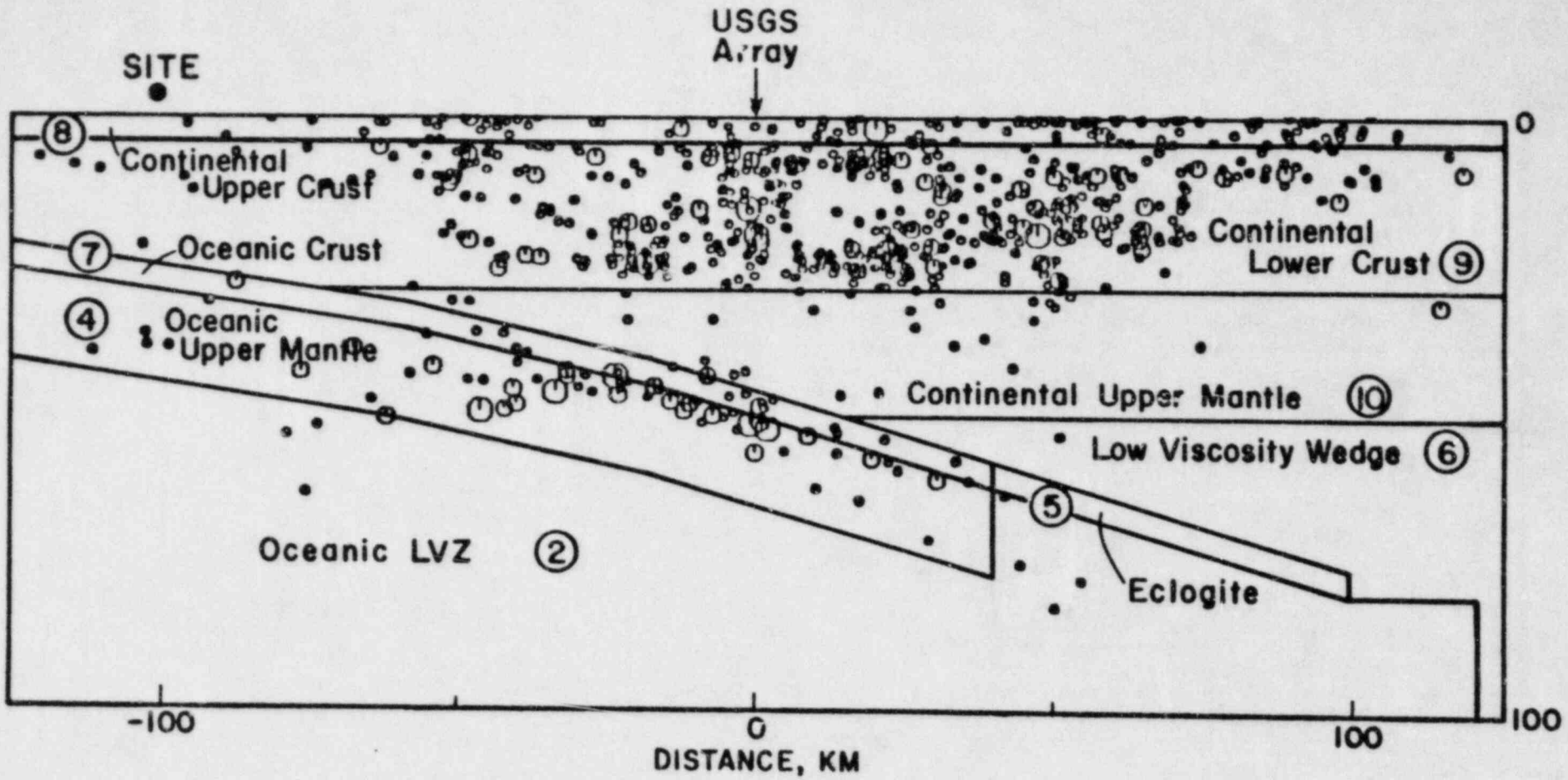
USGS
Array
SITE
8
Continental
Upper Crust
7
Oceanic Crust
4
Oceanic
Upper Mantle
Continental
Lower Crust
9
Continental Upper Mantle
10
Low Viscosity Wedge
6
5
Oceanic LVZ
2
Eclogite
0
-100
0
100
100
DISTANCE, KM

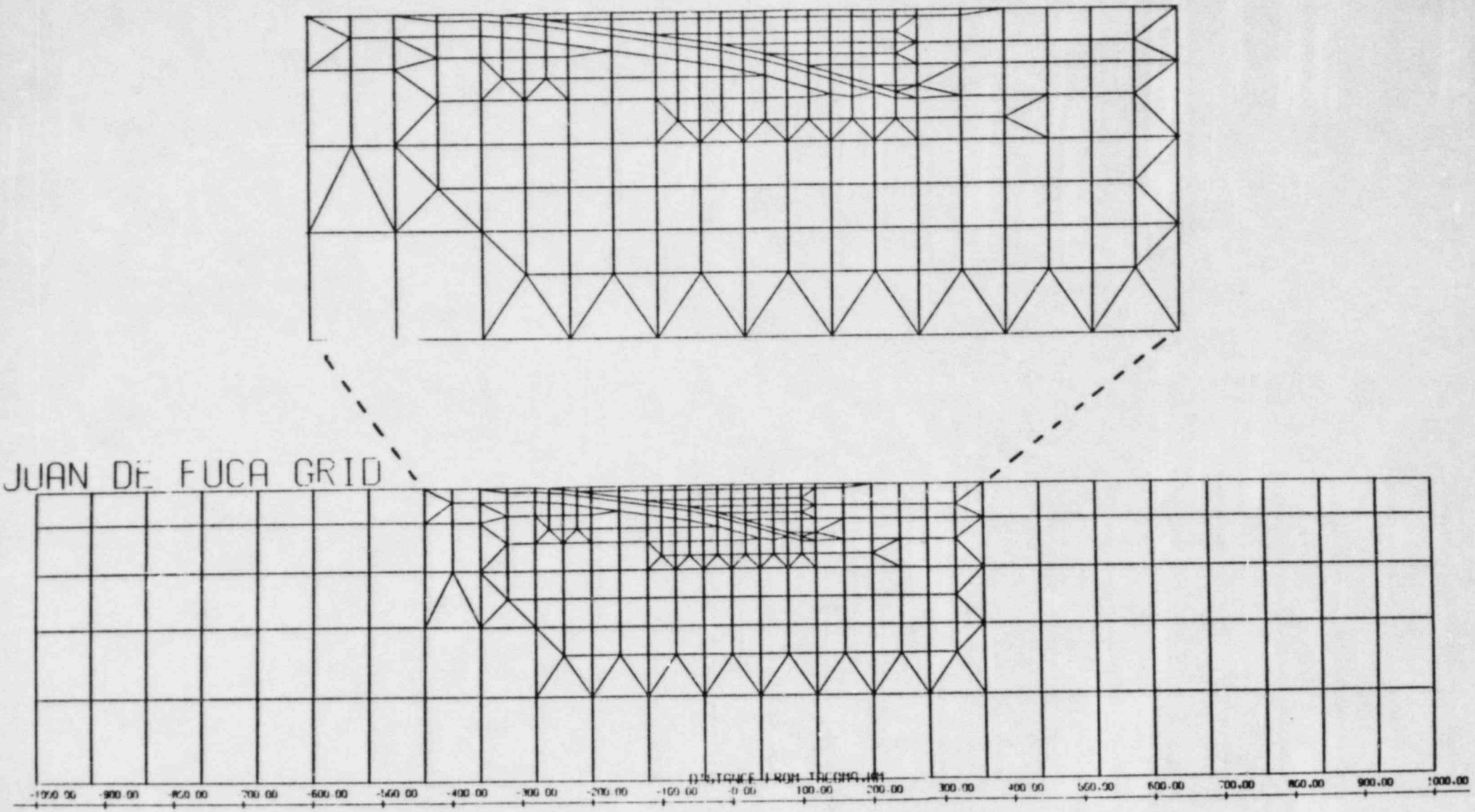
JUAN DE FUCA GRID
-1000.00
-900.00
-800.00
-700.00
-600.00
-500.00
-400.00
-300.00
-200.00
-100.00
-0.00
100.00
200.00
300.00
400.00
500.00
600.00
700.00
800.00
900.00
1000.00

Fig 3

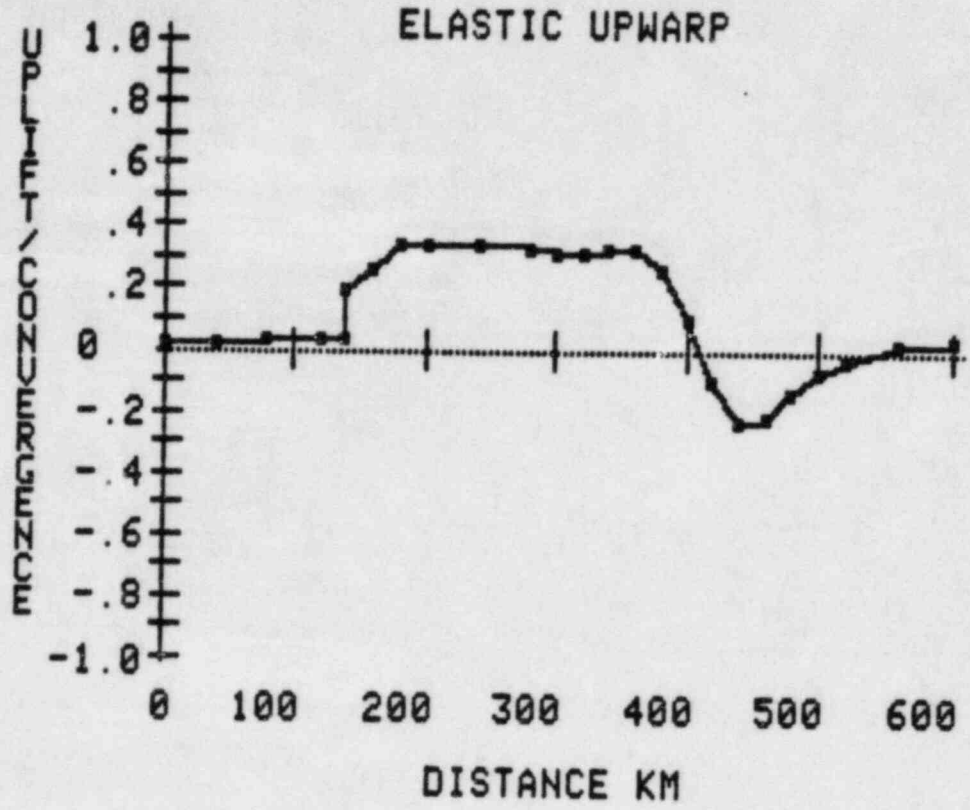
ELASTIC UPWARP
UPLIFT/DOWNWARP
1.0
.8
.6
.4
.2
0
-.2
-.4
-.6
-.8
-1.0
0
100
200
300
400
500
600
DISTANCE KM

Fig. 4

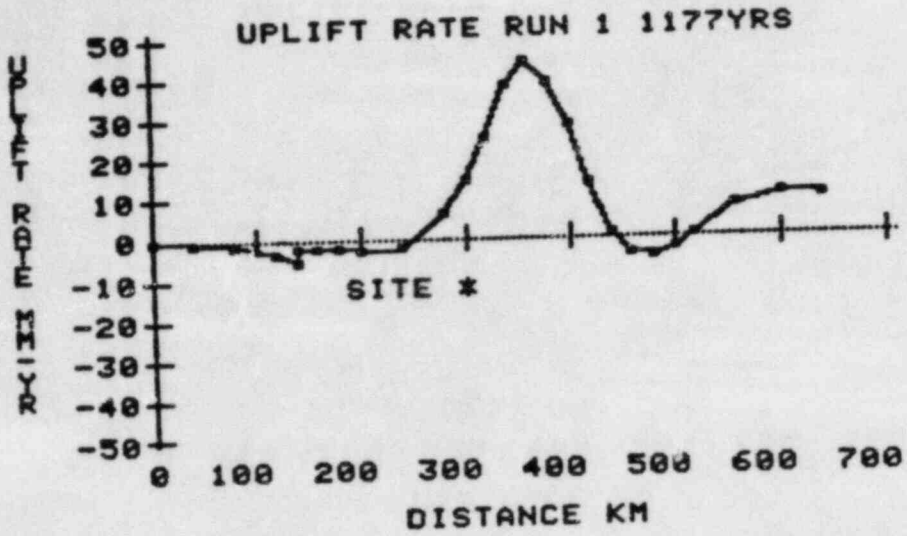
UPLIFT RATE RUN 1 1177YRS
UPLIFT RATE MM-YR
50
40
30
20
10
0
-10
-20
-30
-40
-50
SITE *
0
100
200
300
400
500
600
700
DISTANCE KM

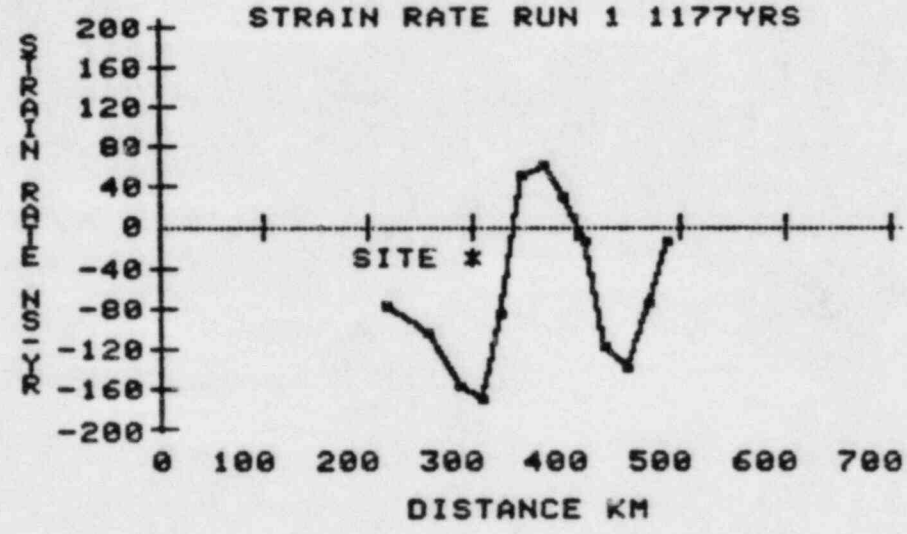
STRAIN RATE RUN 1 1177YRS
STRAIN RATE NS-YR
200
160
120
80
40
0
-40
-80
-120
-160
-200
SITE *
0
100
200
300
400
500
600
700
DISTANCE KM

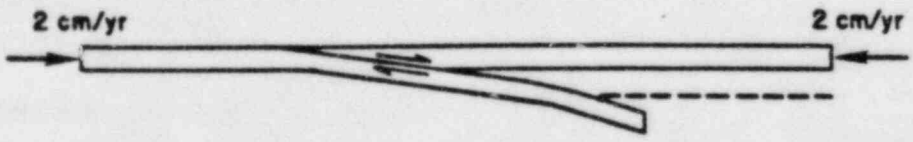
2 cm/yr
2 cm/yr

Fig 5

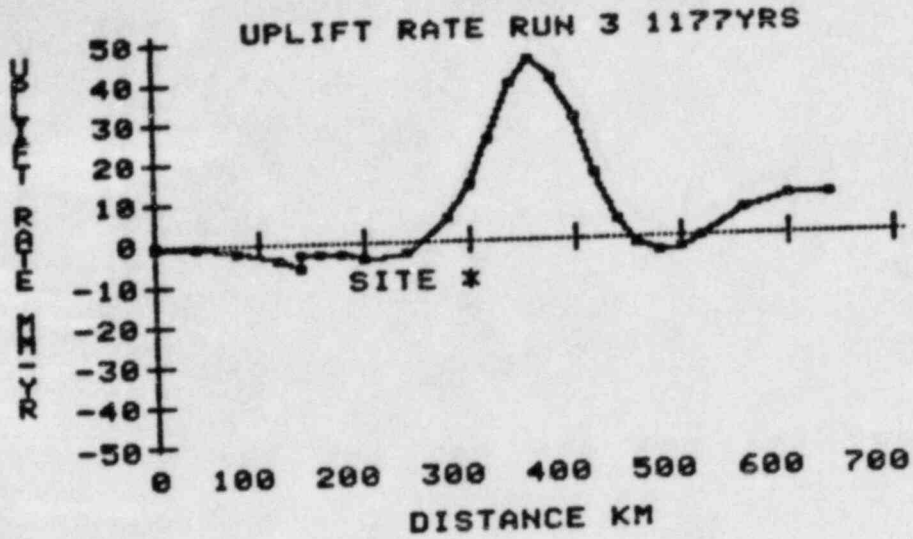
UPLIFT RATE RUN 3 1177YRS
UPLIFT RATE MM-YR
50
40
30
20
10
0
-10
-20
-30
-40
-50
SITE *
0 100 200 300 400 500 600 700
DISTANCE KM

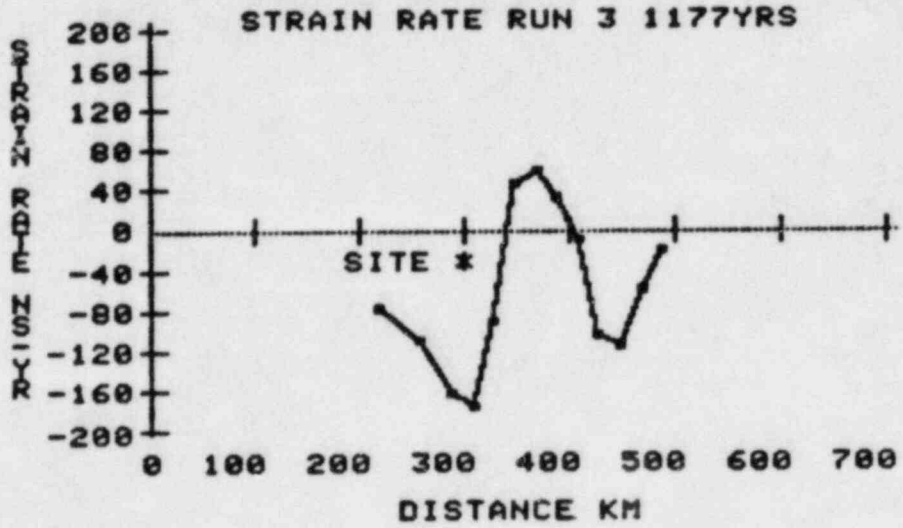
STRAIN RATE RUN 3 1177YRS
STRAIN RATE NS-YR
200
160
120
80
40
0
-40
-80
-120
-160
-200
SITE *
0 100 200 300 400 500 600 700
DISTANCE KM

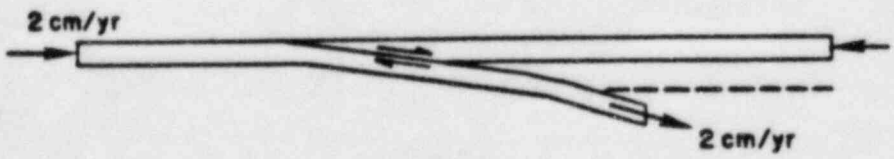
2 cm/yr
2 cm/yr

Fig. 6

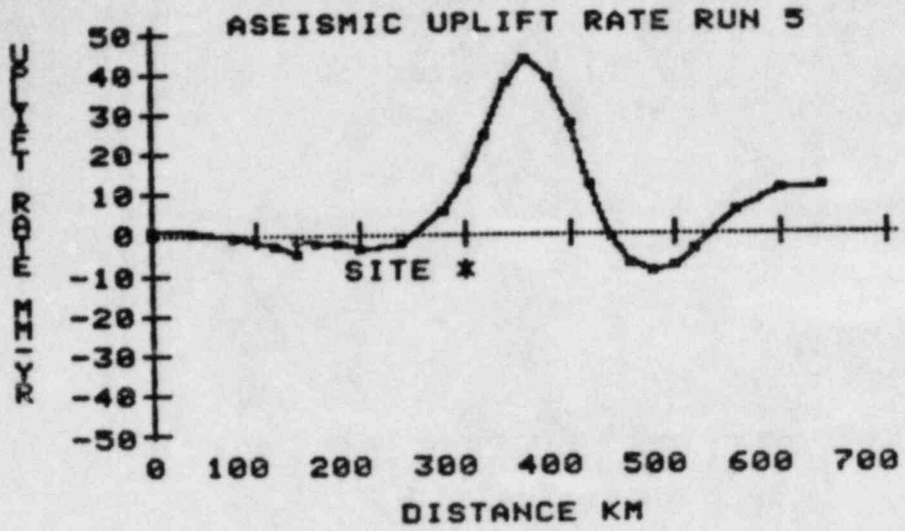
ASEISMIC UPLIFT RATE RUN 5
UPLIFT RATE MM/YR
50
40
30
20
10
0
-10
-20
-30
-40
-50
SITE *
0 100 200 300 400 500 600 700
DISTANCE KM

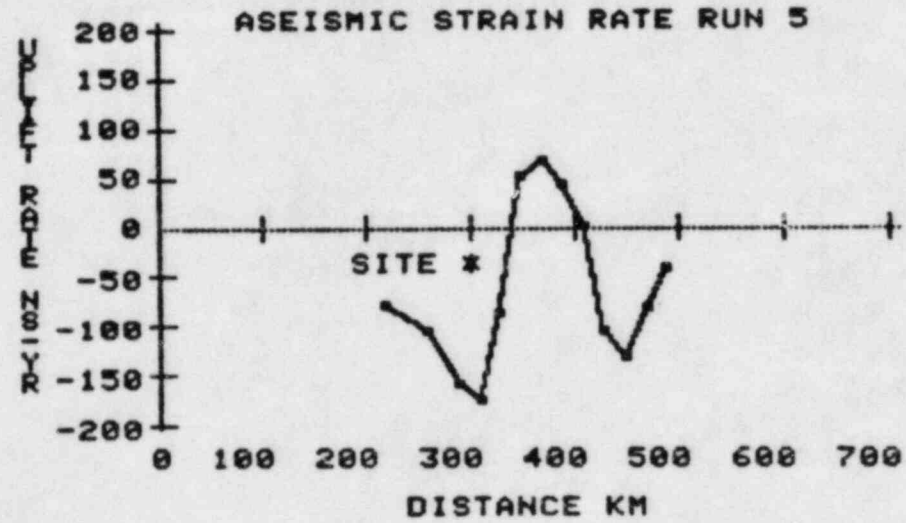
ASEISMIC STRAIN RATE RUN 5
UPLIFT RATE NS/YR
200
150
100
50
0
-50
-100
-150
-200
SITE *
0 100 200 300 400 500 600 700
DISTANCE KM

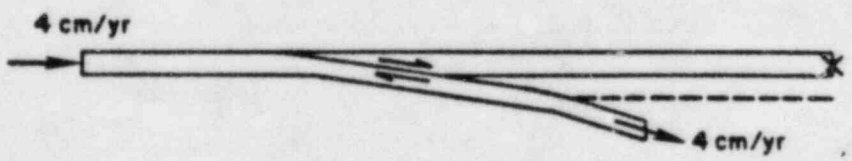
4 cm/yr
4 cm/yr

Fig. 7

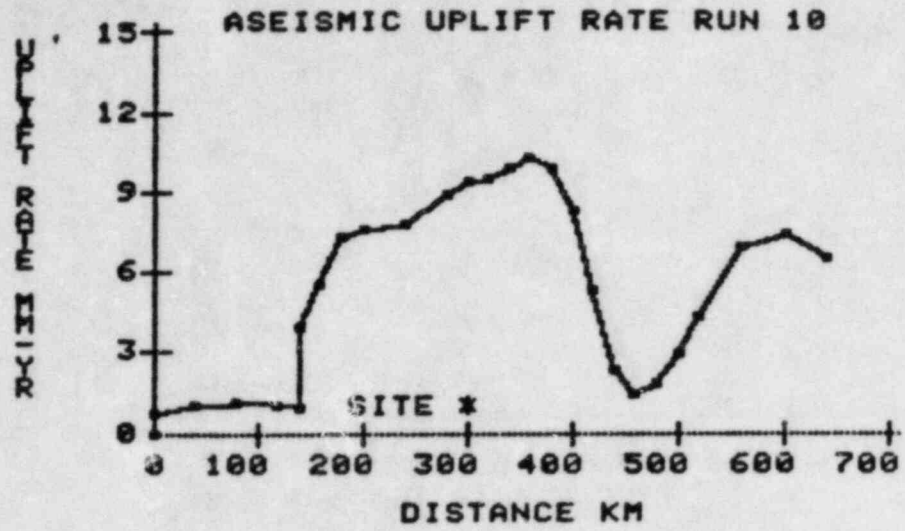
ASEISMIC UPLIFT RATE RUN 10
UPLIFT RATE MM/YR
15
12
9
6
3
0
SITE *
0 100 200 300 400 500 600 700
DISTANCE KM

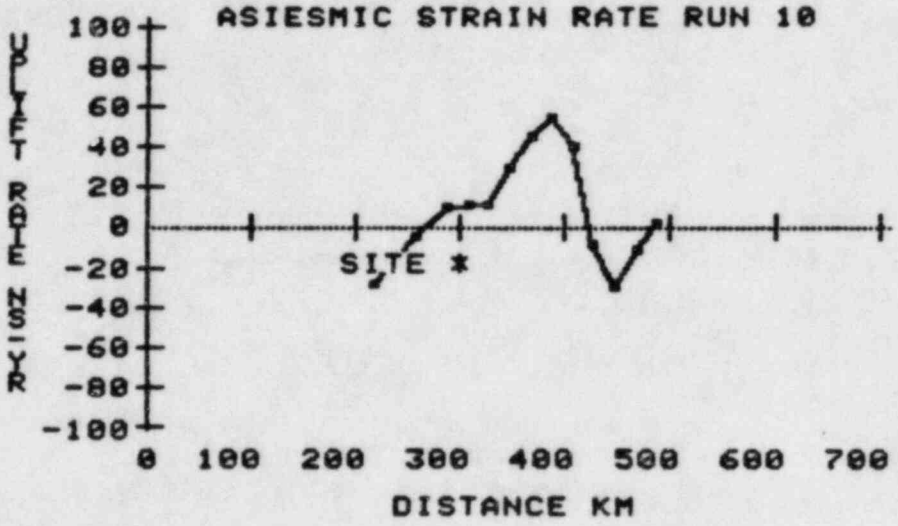
ASIESMIC STRAIN RATE RUN 10
UPLIFT RATE NS/YR
100
80
60
40
20
0
-20
-40
-60
-80
-100
SITE *
0 100 200 300 400 500 600 700
DISTANCE KM

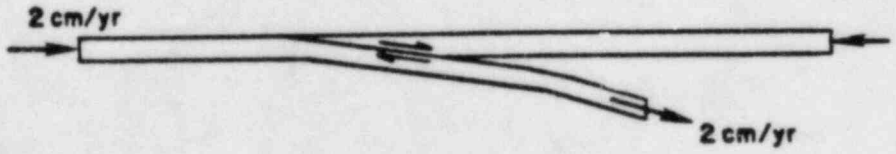
2 cm/yr
2 cm/yr

Fig. 8

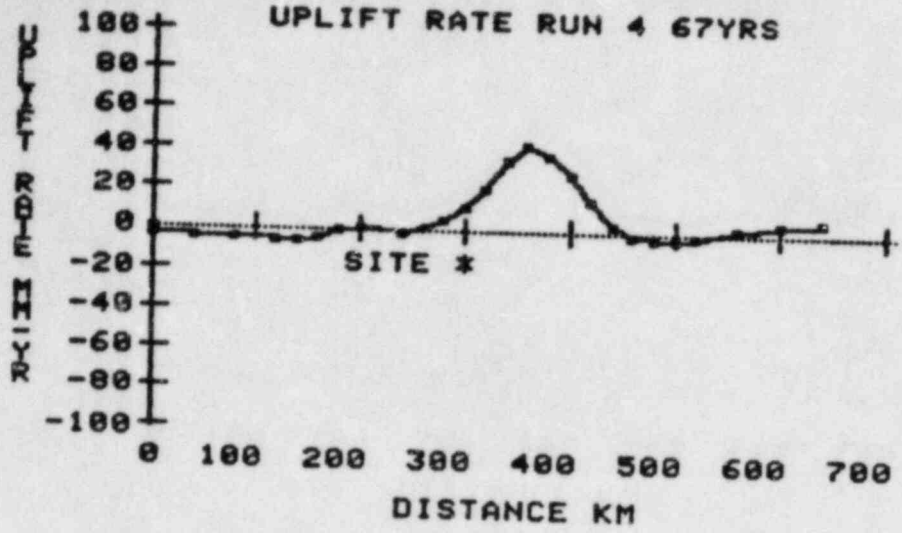
UPLIFT RATE RUN 4 67YRS
UPLIFT RATE MM-YR
100
80
60
40
20
0
-20
-40
-60
-80
-100
SITE *
0 100 200 300 400 500 600 700
DISTANCE KM

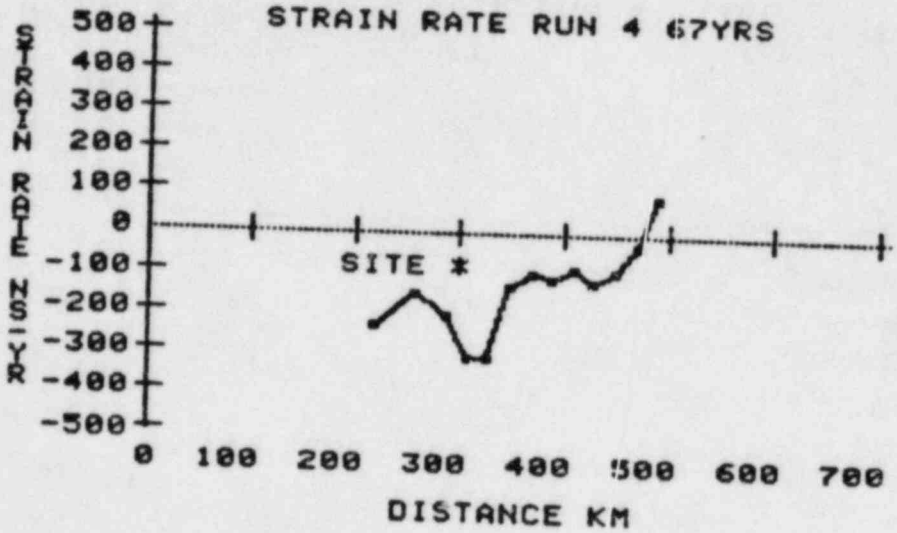
STRAIN RATE RUN 4 67YRS
STRAIN RATE NS-YR
500
400
300
200
100
0
-100
-200
-300
-400
-500
SITE *
0 100 200 300 400 500 600 700
DISTANCE KM

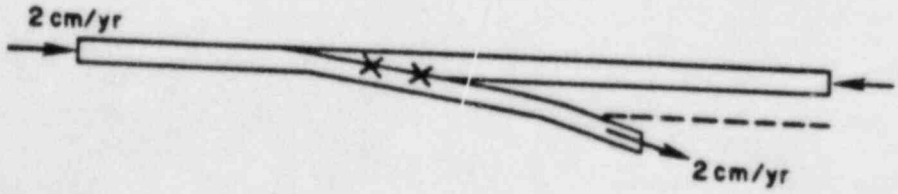
2 cm/yr
2 cm/yr

Fig. 9

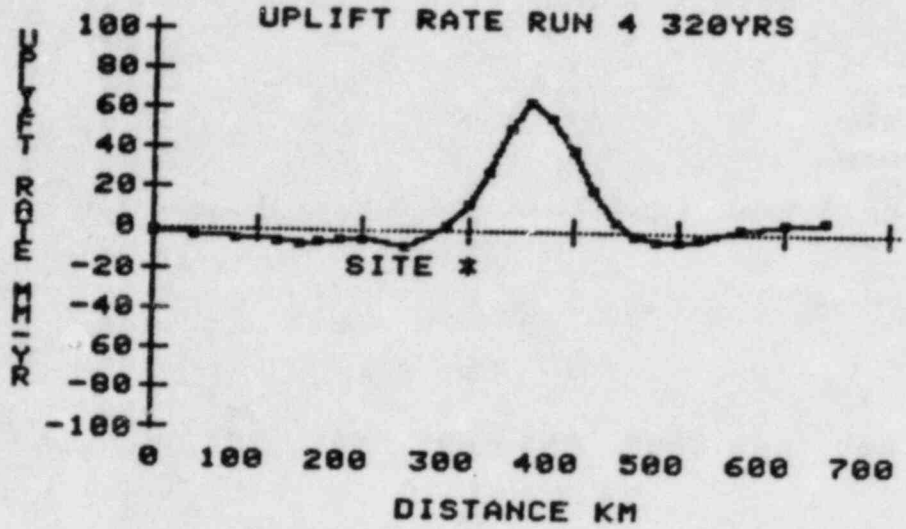
UPLIFT RATE RUN 4 320YRS
UPLIFT RATE MM-YR
100
80
60
40
20
0
-20
-40
-60
-80
-100
SITE *
0 100 200 300 400 500 600 700
DISTANCE KM

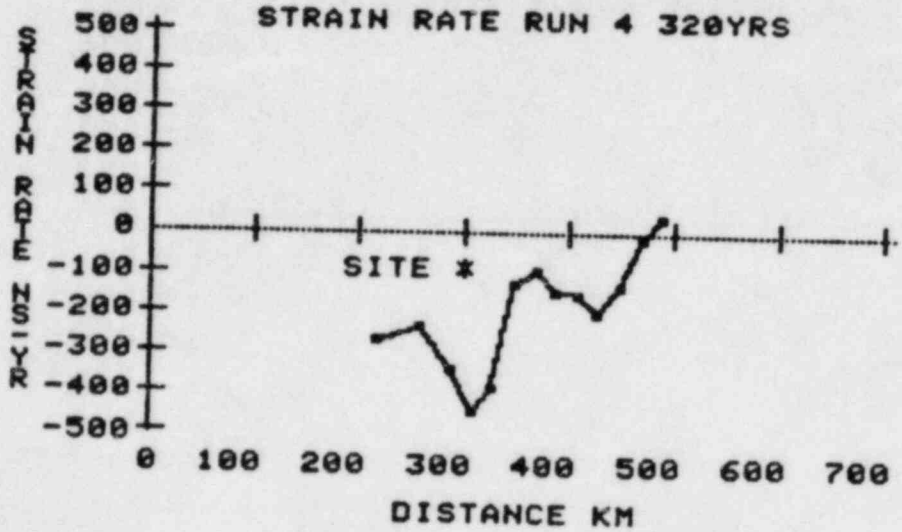
STRAIN RATE RUN 4 320YRS
STRAIN RATE NS-YR
500
400
300
200
100
0
-100
-200
-300
-400
-500
SITE *
0 100 200 300 400 500 600 700
DISTANCE KM

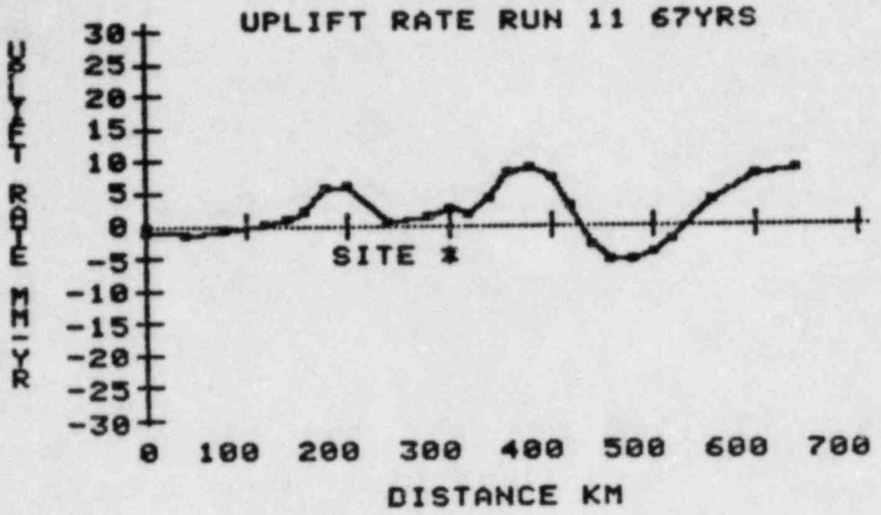
UPLIFT RATE RUN 11 67YRS
UPLIFT RATE MM-YR
30
25
20
15
10
5
0
-5
-10
-15
-20
-25
-30
SITE
0
100
200
300
400
500
600
700
DISTANCE KM

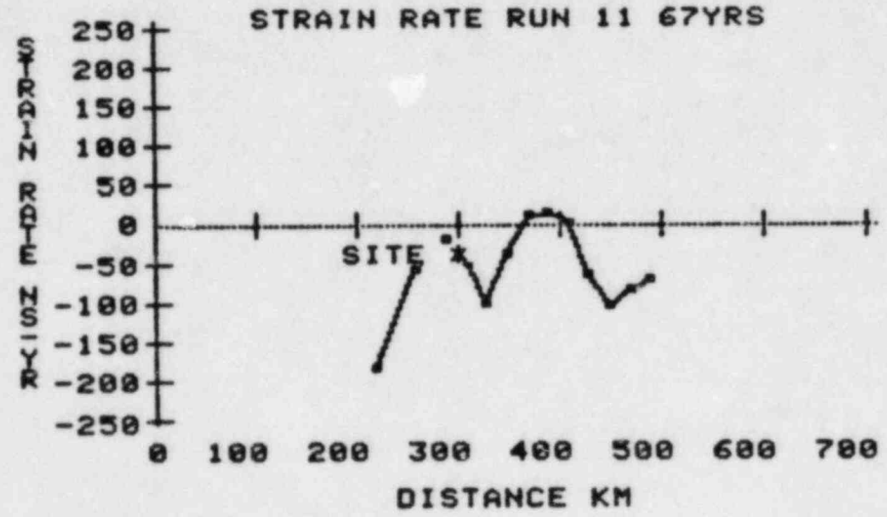
STRAIN RATE RUN 11 67YRS
STRAIN RATE NS-YR
250
200
150
100
50
0
-50
-100
-150
-200
-250
SITE
0
100
200
300
400
500
600
700
DISTANCE KM

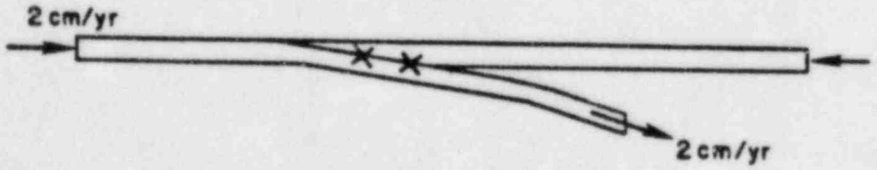
2 cm/yr
2 cm/yr

Fig. 11

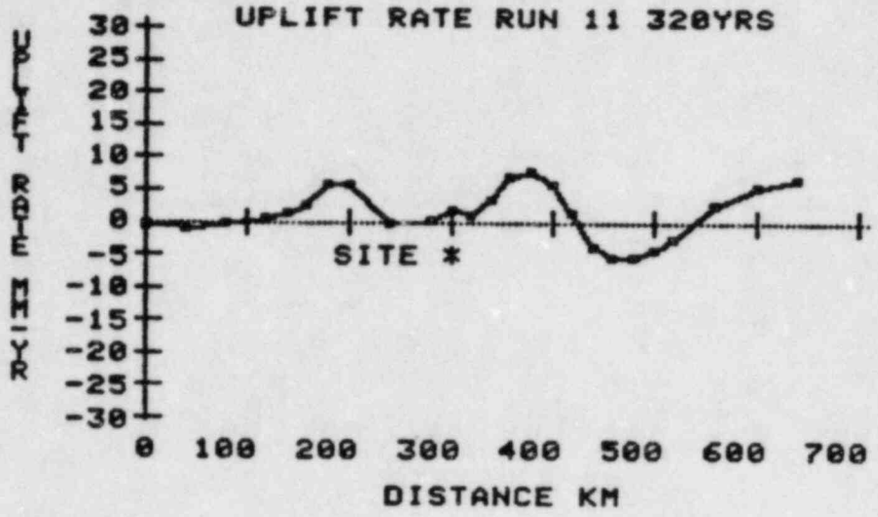
UPLIFT RATE RUN 11 320YRS
UPLIFT RATE MM-YR
30
25
20
15
10
5
0
-5
-10
-15
-20
-25
-30
SITE *
0 100 200 300 400 500 600 700
DISTANCE KM

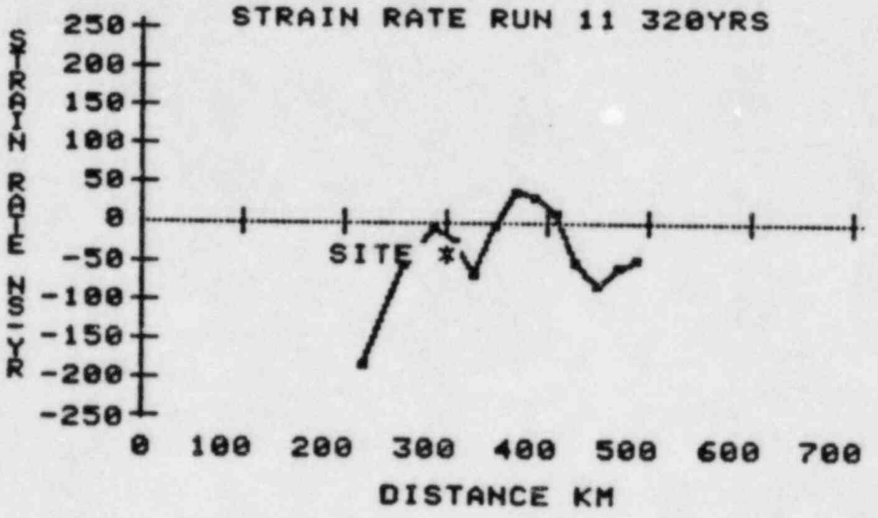
STRAIN RATE RUN 11 320YRS
STRAIN RATE NS-YR
250
200
150
100
50
0
-50
-100
-150
-200
-250
SITE *
0 100 200 300 400 500 600 700
DISTANCE KM

Fig 12

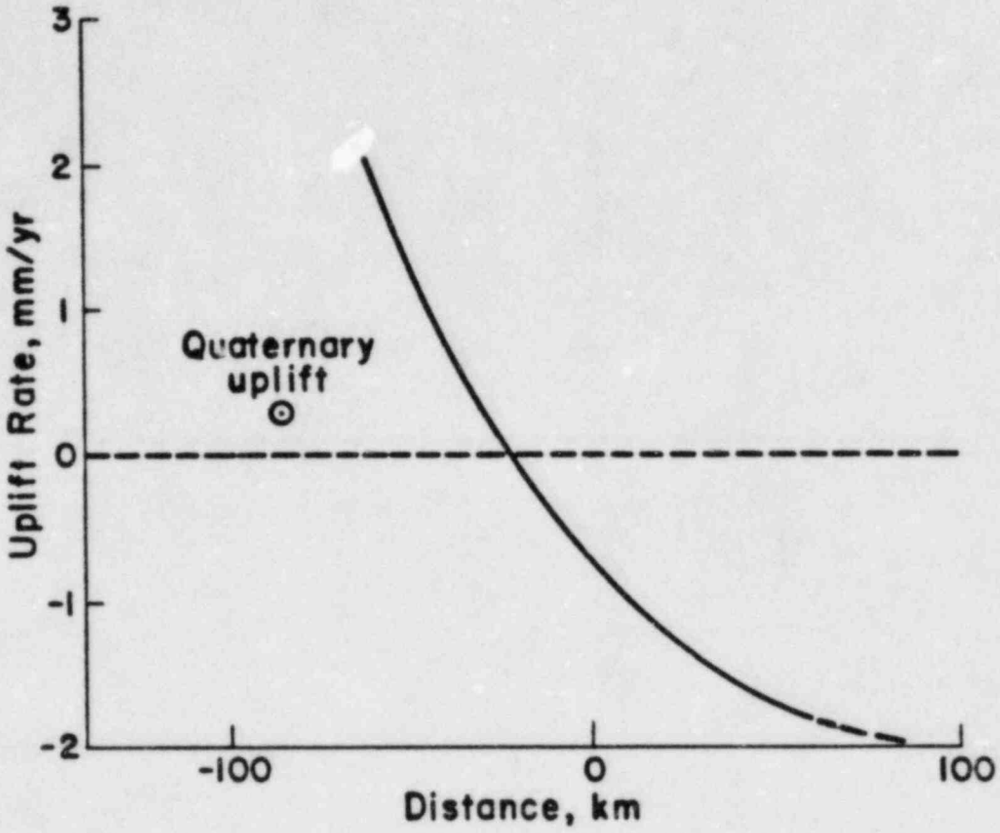
3
2
1
0
-1
-2
Uplift Rate, mm/yr
Quaternary
uplift
-100
0
100
Distance, km

Fig 13